

The Onset of Matter-Wave Amplification in a Superradiant Bose-Einstein Condensate

Dominik Schneble,* Yoshio Torii,† Micah Boyd, Erik W. Streed, David E. Pritchard, Wolfgang Ketterle

The interaction of short and strong laser pulses with an atomic Bose-Einstein condensate is found to generate patterns of recoiling atoms that are different from those seen in previous light-scattering experiments. This phenomenon can only be explained by optical stimulation, showing that the previous description of superradiance as atomic stimulation is incomplete and that matter-wave amplification in Bose-Einstein condensates is suppressed at short times. Our experiments clarify the nature of bosonic stimulation in the four-wave mixing of light and atoms.

Superradiance is the collective emission of light from an ensemble of excited atoms and involves the spontaneous buildup of coherence in a macroscopic ensemble of atoms. Dicke, in his seminal work (1), showed that the spontaneous emission of photons from an ensemble of N localized atoms is enhanced by a factor of N over the single-atom emission rate when the atoms are in a cooperative state with all the transition moments in phase. If, however, the atomic ensemble extends over more than the wavelength of the radiation, the situation becomes more complex. Superradiant emission is then only possible along certain directions where a phase-matching condition is fulfilled. Furthermore, there are now two physically distinct pictures of the collective emission process in which the distinction between spontaneous emission and stimulated emission is blurred (2). In the viewpoint introduced by Dicke, the entire extended ensemble interacts with empty modes of the electromagnetic field, and all photons are emitted spontaneously, albeit in a cooperative way. In the other picture, some atoms emit spontaneously, and this radiation stimulates other atoms to emit in phase. The equivalence of these two pictures emphasizes that, if a system emits many photons cooperatively, a strict distinction between spontaneous and stimulated emission is no longer possible. The phenomenon of superradiance thus deepens and clarifies our understanding of the interaction of matter and light.

Because of their coherent nature, Bose-Einstein condensates readily exhibit collective superradiant behavior. Controversy re-

garding the role of quantum statistics in superradiance was resolved in (3, 4) in which it was shown that processes attributed to bosonic stimulation can also be expected in superradiant Fermi systems. An important application of superradiance has been the coherent amplification of matter waves (5, 6). We study superradiance in the short-pulse limit and show that amplification is attenuated at short times, leading to a more profound understanding of matter-wave amplification.

When a Bose-Einstein condensate is illuminated by a single laser beam (pump beam), light can be scattered into an empty mode. The condensate at rest, “dressed” by the pump beam, corresponds to the excited electronic state in the usual superradiance. Spontaneous emission is now replaced by a spontaneous Rayleigh scattering process that leads to a recoiling atom. This atom interferes with the atoms at rest and creates a periodic density modulation that, in turn, leads to an increase of the scattering rate, thus amplifying itself. Because the square of the density modulation is proportional to the number of recoiling atoms, one can describe this process as matter-wave amplification due to bosonic stimulation by atoms (5–7). Here, superradiance corresponds to the diffraction of the pump beam from a matter-wave grating in the condensate volume. In an elongated condensate, the gain is strongest when the photons leave the condensate along its long axis in the so-called endfire mode (1), whereas the atoms recoil at an angle of 45° with respect to the axis and emerge as a distinct atomic cloud (forward peak) with a momentum component parallel to the pump beam. The theoretical literature on superradiant scattering in condensates (5, 7–12) corroborates this description, but here we show that it is incomplete.

Our new experimental results suggest an alternative picture for superradiance in which the endfire beam and the pump beam form an optical standing wave and diffract atoms in a

stimulated scattering process between momentum states. The ambiguity between spontaneous and stimulated emission now reappears as the ambiguity of whether light is diffracted from a matter-wave grating or whether atoms are diffracted from a light grating. In the latter picture, the forward peaks in superradiance correspond to Bragg diffraction of atoms (13, 14). In the present work, we observed the diffraction of atoms into additional states with momentum components antiparallel to the pump beam (backward peaks). This is possible in the regime of short pulses in which several recoil states are quasi-degenerate [Kapitza-Dirac diffraction (15, 16)]. The backward peaks result from the reabsorption of spontaneously scattered photons and stimulated emission back into the pump beam. This off-resonant process, which cannot be described by the Dicke picture of collective spontaneous emission, both limits the growth of the endfire mode and suppresses matter-wave amplification by destructive interference.

The experiments discussed here were performed with a ^{87}Rb condensate in the $|F = 1, m_F = -1\rangle$ hyperfine ground state, where F and m_F are the quantum numbers for the total spin and its z component, respectively. We collected 10^{10} atoms in a magneto-optical trap from a slow atomic beam with a flux of 10^{11} s^{-1} . The atoms were cooled further in dark optical molasses and evaporatively cooled in a cloverleaf-type Ioffe-Pritchard magnetic trap. The trapped, almost-pure condensates contained about two million atoms and had Thomas-Fermi radii of $100 \mu\text{m}$ and $7.5 \mu\text{m}$ along the axial and radial directions, respectively. To induce superradiant scattering, we illuminated the condensate with an off-resonant pump laser beam (center intensity of 63 m W cm^{-2} and e^{-2} radius of 1.6 mm) for a variable pulse duration τ . The linearly polarized beam was incident horizontally along a radial direction with its electric field vector perpendicular to the axial direction (compare Figs. 1 and 2A). Immediately after applying the laser pulse, the atomic momentum distribution was analyzed by switching off the magnetic trap and imaging the atomic ensemble after 30 ms of ballistic expansion. Absorption images were obtained with the use of a vertical probe beam after the atoms had been optically pumped into the $F = 2$ ground state (Fig. 1). In case A for short pulses, the Rayleigh scattering rate Γ_{sc} was chosen to be comparable to the single-photon recoil frequency $\omega_r = 2.4 \times 10^4 \text{ s}^{-1}$ so that a large fraction of condensate atoms were scattered on a time scale that was short compared to the recoil time $\omega_r^{-1} = 42 \mu\text{s}$. In this case, we observed a nearly symmetric, X-shaped pattern. For comparison, when the detuning was chosen to be one order of magnitude larger (case B), the pattern evolved on

Massachusetts Institute of Technology—Harvard Center for Ultracold Atoms, Research Laboratory of Electronics and Department of Physics, Massachusetts Institute of Technology, Cambridge, MA 02139, USA.

*To whom correspondence should be addressed. E-mail: schneble@mit.edu

†Present address: Department of Physics, University of Tokyo, 3-8-1 Komaba, Meguro-Ku, Tokyo, Japan.

REPORTS

a time scale that was one order of magnitude above the recoil time, and the familiar super-radiant scattering fan appeared, as in (8).

The scattering processes that give rise to the observed symmetric pattern are illustrated in Fig. 2A. In lowest order, forward peaks [label (1)] are generated when a pump photon with momentum $\hbar\mathbf{k}$ is scattered off a condensate atom (zero momentum), thereby producing a scattered photon with momentum $\hbar(\mathbf{k} - \mathbf{q})$ and a recoiling atom with momentum $\hbar\mathbf{q}$, $q = \sqrt{2}k$. In contrast, backward peaks [label (2)] are produced when a previously scattered photon is scattered back into the pump mode, thereby transferring a condensate atom into a recoiling atom with momentum $-\hbar\mathbf{q}$. Whereas in the first case energy is conserved, the energy mismatch in the latter case is twice the recoil energy, $\Delta E = 4\hbar\omega_r$. Therefore this process can only take place as long as the energy uncertainty $\hbar/\tau > \Delta E$, that is, for pulse lengths τ up to $\sim 10 \mu\text{s}$. At an early stage, when the endfire modes do not yet dominate completely, one can clearly recognize the dipole pattern of spontaneous photon emission (Fig. 2B) as a halo of recoiling atoms with radius $\hbar k$ on the right-hand side of the condensate. In addition, one also observes another halo on the left-hand side. This halo results from stimulated scattering of the spontaneously emitted photons back into the pump laser beam.

Fig. 1. Superradiant scattering of a laser beam (arrow) from a Bose-Einstein condensate in the short-pulse (A) and long-pulse (B) limit. Absorption images of the atomic density distribution were taken after 30 ms of ballistic expansion. In case A, Δ was -420 MHz and τ was $6 \mu\text{s}$. In case B, Δ was -4400 MHz and τ was $800 \mu\text{s}$. The inset in (B) is a magnification of the region around the condensate showing depletion of its center; for better visibility the contrast has been enhanced by a factor of 1.5. Also shown is a profile of the average optical density in the center region. The field of view of both images is 2.0 mm by 2.0 mm , and that of the inset is $120 \mu\text{m}$ by $270 \mu\text{m}$.

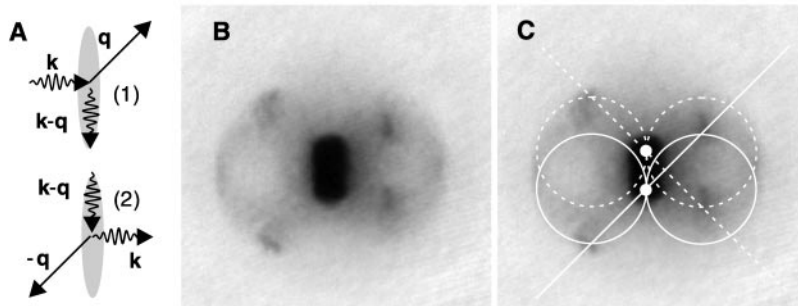
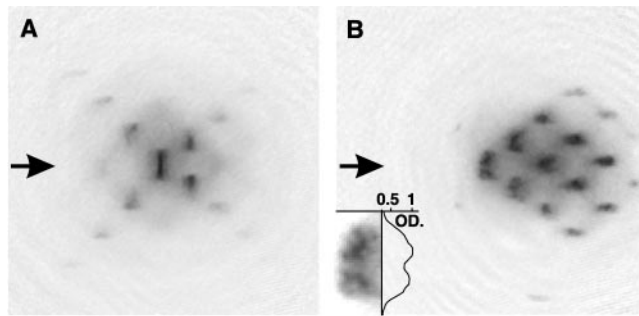


Fig. 2. Scattering processes (A) and scattering pattern (B) for a short ($\tau = 3 \mu\text{s}$) light pulse. The circles and lines in (C) illustrate the origin of the dipole emission halos and the Kapitza-Dirac diffraction orders.

It is important to notice the slight left-right asymmetry of the X-shaped scattering pattern of Fig. 1A. There exist two endfire modes, q_+ and q_- , propagating in opposite directions due to the axial symmetry of the condensate, and therefore both the backward and forward peaks are grouped in pairs. However, the separation of the backward peaks in the axial direction is larger than that of the forward peaks. This suggests that the scattering processes for each of the two endfire modes occur near the edges of the condensate (Fig. 2C) (17).

This observation allows one to distinguish the two simple pictures in which light is diffracted from atoms or atoms are diffracted from light. The fact that the scattering process is strongest near the edges of the condensate suggests that atoms are diffracted from an optical standing wave formed by the pump and endfire modes: The intensity of the endfire modes and thus the intensity of the standing wave are highest near the edges of the condensate. Conversely, if the scattering processes could simply be described by diffraction of light from a matter-wave grating, one would expect the recoiling atoms to originate in the center where the atomic density and the diffraction efficiency of the grating are highest. This is indeed the case in the long-pulse limit where the Thomas-Fermi profile of the condensate shows depletion in the center (inset of Fig. 1B).

A more detailed analysis of the observed recoil patterns confirms the picture of optical diffraction. For short times $\omega_r\tau \ll 1$, one can neglect the frequency difference between the pump light ($+y$ direction) and the endfire modes ($\pm z$ direction), and their interference leads to a modulated light intensity

$$I_{\text{mod}} = 2E_k E_{k-q_+} \cos k(y+z) + 2E_k E_{k-q_-} \cos k(y-z) + E_{k-q_+} E_{k-q_-} \cos 2kz \quad (1)$$

where E_{k-q_+} and E_{k-q_-} are the field amplitudes of the two endfire modes with wavevectors $k - q_+$ and $k - q_-$, respectively, and E_k is the amplitude of the pump beam. The first and second terms give rise to diffraction of atoms into momenta $\hbar q_n = n\sqrt{2}\hbar k$ along axes tilted at $\pm 45^\circ$ with respect to the long axis, with populations (15)

$$P_n = J_n^2(\Omega_{2R}\tau), \quad n = 0, \pm 1, \pm 2, \dots \quad (2)$$

Here the J_n are Bessel functions of the first kind; $\Omega_{2R} = \omega_{R,k} \omega_{R,k-q_i} / 2\Delta$ is the two-photon Rabi frequency, given by the Rabi frequencies $\omega_{R,k}$ and $\omega_{R,k-q_i}$ ($i = +, -$) of the laser beam and the two endfire modes; and Δ is the detuning of the beams. Scattering processes that involve more than one endfire mode (such as those induced by the third term in Eq. 1) can be neglected as long as the endfire mode intensities are smaller than the intensity of the pump mode.

With the use of this model, we can determine the intensity of the individual endfire modes. Above $5 \mu\text{s}$, the population in the minus-second-order peak exceeds 50% of that in the minus-first-order peak. At $6 \mu\text{s}$, the ratio is 63%, which implies a two-photon Rabi frequency $\Omega_{2R} = 3.9 \times 10^5 \text{ s}^{-1}$ corresponding to an endfire-mode intensity of 0.8 m W cm^{-2} . This intensity is more than two orders of magnitude larger than the intensity of spontaneous Rayleigh scattering into this mode (18).

A comparison of an extracted pattern to a calculated Kapitza-Dirac pattern is given in Fig. 3B. There is good general agreement; however, a major discrepancy exists for the zeroth order, that is, for the condensate itself. The depletion of the condensate is far less than predicted by the model. This is easily explained by the fact that the scattering processes take place mainly near the edges, leaving many condensate atoms in the central region. The model assumes an external endfire laser beam, whereas the endfire mode is produced in the condensate volume itself. Another discrepancy appears at longer times when τ approaches the two-photon recoil time: The resonant first-order peak $p_1 = \sqrt{2}\hbar k$ becomes dominant. The emergence of this asymmetry is a clear signature for the transition from the Kapitza-Dirac to the Bragg regime, that is, for the onset of energy conservation.

Before discussing the interplay between optical and atomic stimulation in our short-pulse experiment, we want to emphasize the qualitative equivalence of these two pictures in the long-pulse limit. The superradiant gain has been successfully interpreted as matter-wave stimulation (7, 8), that is, as the diffraction of photons from a self-amplifying matter-wave grating. However, by extrapolating the observed short-time behavior to longer times, a purely optical interpretation of superradiance emerges: The endfire modes and the pump beam form a standing light wave from which the atoms can diffract. For $\omega_r \tau \gg 1$, the stimulated backscattering of endfire mode photons into the pump beam is energetically suppressed, the endfire mode grows exponentially in time, and so does the diffraction efficiency of the standing light wave. In this interpretation, superradiance in the long-pulse limit is nothing but (self-stimulated) Bragg scattering.

The equivalence of the two descriptions in the long-pulse limit can be obtained in a more quantitative way by considering the rate for Bragg scattering from the standing light wave formed by the pump beam and an endfire mode (neglecting propagation effects) (7):

$$W_B = N\Omega_{2R}^2/\Gamma_2 \quad (3)$$

Here N is the number of atoms in the condensate, and Γ_2 is the width of the Bragg resonance (19). The Rabi frequency of the pump beam can be expressed through its Rayleigh scattering rate Γ_{sc} as $\omega_{R,k} = 2\Delta(\Gamma_{sc}/\Gamma)^{1/2}$, where Γ is the natural linewidth. The number of photons scattered in the coherence time $1/\Gamma_2$ is identical to the number of recoiling atoms N_q inside the condensate volume. This gives the Rabi frequency of the endfire mode as $\omega_{R,k-q} = \Gamma[N_q\Gamma_2\hbar\omega/(2I_s A)]^{1/2}$, where $I_s = \pi\hbar\omega\Gamma/3\lambda^2$ is the saturation intensity and A is the cross-sectional area of the condensate (λ is the wavelength, and ω is the frequency of the transition). The result

$$W_B = \Gamma_{sc} \frac{3}{2\pi} \frac{\lambda^2}{A} NN_q \equiv GN_q \quad (4)$$

is, up to a numerical factor, identical to the result for the superradiant gain coefficient G obtained in (8), in which the interference term NN_q was interpreted as the modulation depth of the matter-wave grating from which the pump photons diffract.

This equivalence between optical and atomic stimulation was not properly recognized in earlier treatments (7, 8) that were based on the argument that the number of photons in the condensate volume was smaller than one. However, as already pointed out in (7), the relevant photons (and recoiling atoms) are all those produced within the coherence time $1/\Gamma_2$. Although for the atoms the relevant mode volume is given by the condensate itself, it is much bigger for the

scattered photons because the coherence length of the endfire mode greatly exceeds the length of the condensate. The fact that photons and recoiling atoms are produced in pairs implies that their effective numbers are equal and that atomic stimulation in one picture can be replaced by optical stimulation in another picture.

We now apply these concepts to the short-pulse limit. At early times τ , the scattering pattern is symmetric, and therefore the creation of endfire-mode photons (positive orders or forward peaks) is as probable as their absorption (negative orders or backward peaks), resulting in a fully suppressed superradiant gain. Spontaneous Rayleigh scattering is only amplified at longer times when the pattern develops an asymmetry. We describe this by attributing a Lorentzian lineshape with a linewidth $\Gamma \propto 1/\tau$ to the first and minus-first order (neglecting coherences). The former is resonant, and the latter is detuned by the two-photon recoil shift $\delta = \Delta E/\hbar$. This model predicts a suppression of the gain by a factor of $(2\delta/\Gamma)^{-2} \propto (\delta\tau)^{-2}$. With the use of a coherent model based on driven two-level systems, we find a suppression by a factor of $12(\delta\tau)^{-2}$, which has the same quadratic time dependence. The suppression of the gain at short times can also be understood in a purely atomic picture. An optical standing wave creates a phase grating in the atomic cloud, which transforms into a density grating only after the inverse recoil frequency, that is, the time it takes the atoms to move half a wavelength. For a given number of recoiling atoms, the atomic gain is initially zero and grows as $(\delta\tau)^2$, in agreement with the picture of optical amplification. It is the matter wave grating that gets amplified, rather than the number of recoiling atoms itself: The density grating created by the population N_q destructively interferes with the population N_{-q} in the backward peak, and the gain is reduced.

Although all three models are qualitative, they consistently predict a suppression of the gain by around two orders of magnitude for pulse lengths around 1 μ s. For the typical condensate geometry in (8) and the present experiment, the ratio of G as defined in Eq. 4 to Γ_{sc} is about 4×10^3 . At $\tau \approx 1$ μ s, we expect an (attenuated) gain coefficient $G \sim 10^6$ s^{-1} for $\Gamma_{sc} \approx \omega_r$. The observed magnitude for the endfire-mode intensity is consistent with such a low gain. The attenuation is also evident when the scattering rate for the first order, $N_q \sim 10^{10}$ s^{-1} , is compared to the global Rayleigh scattering rate of the pump beam. In the short-pulse limit, it is of the same order, whereas in the long-pulse limit an enhancement of one order of magnitude was observed (8).

This new physical picture of superradiance at short times can be applied to the atom am-

plifier (5, 6) where a condensate illuminated by a pump beam is seeded with $N_q(0)$ recoiling atoms, resulting in a density grating. This grating diffracts the pump light into the endfire mode. At early times, the density modulation is not amplified because the number of atoms added to mode q is accompanied by an equal number in mode $-q$, and the two additional matter-wave gratings interfere destructively. Therefore, the gain equation is $\dot{N}_q(t) = GN_q(0)$, which implies linear growth. Exponential growth only starts after the inverse recoil frequency, when the atoms in mode $-q$ have disappeared because of energy conservation.

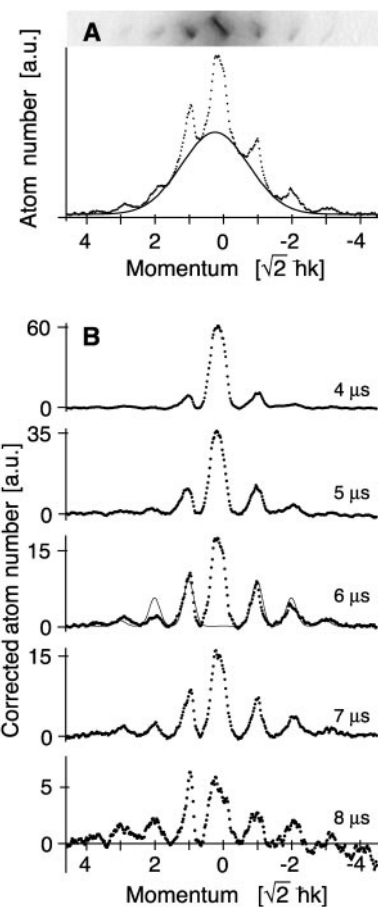


Fig. 3. Comparison of superradiant scattering in the short-pulse regime with Kapitza-Dirac diffraction. (A) The atom numbers in the image of Fig. 1A were integrated over a thin strip that contains the condensate and the diffraction orders. The strip is oriented along the direction from the bottom right to the top left of the image in Fig. 1A. The solid curve is a Gaussian representing the broad background of incoherently scattered and residual thermal atoms. a.u., arbitrary units. (B) Diffraction patterns for pulse durations τ between 4 and 8 μ s. These patterns were obtained by subtracting the background from images similar to those in Fig. 1A. At 6 μ s, the corresponding Kapitza-Dirac pattern for a standing light wave formed by two crossed laser beams with a Ω_{2R} of 3.9×10^5 s^{-1} is shown as a solid line. The widths of the peaks (approximated by Gaussians) were chosen to fit the minus-first-order peak.

In conclusion, by exploring the short-pulse limit of superradiant Rayleigh scattering, we have observed a previously unknown phenomenon in the scattering of a single laser beam by atoms: self-stimulated Kapitza-Dirac diffraction. The symmetry of the diffraction pattern implies a reduced gain for both atom and light amplification at early times. This realizes a novel regime of superradiance in which the atomic system has three almost equally spaced levels with all of the initial population in the middle one. This system has allowed us to illustrate important concepts of stimulation and superradiance. In the Dicke picture, all photons are emitted spontaneously and simply leave the system. However, we directly observed stimulation by and absorption of these photons in the form of Kapitza-Dirac scattering, and therefore the Dicke picture is incomplete for the short-pulse regime. None of the theoretical descriptions of superradiance in Bose-Einstein condensate (5, 7–12) included transitions to momentum states that appear as negative orders in Kapitza-Dirac scattering.

Extrapolating our observations of Kapitza-Dirac scattering to longer pulses establishes the equivalence of self-stimulated Bragg diffraction and matter-wave amplification. There is a widespread opinion that bosonic stimulation is a purely quantum-statistical effect based on symmetry, whereas (3, 4) showed that bosonically enhanced scattering can always be traced back to enhanced fluctuations. Here we have directly shown how photons mediate an effective interaction between the atoms that, after elimination of the photon field, results in bosonic stimulation of atoms. However, at early times, the “stimulating effect” of the population in mode q interferes destructively with the effect of atoms in mode $-q$ and the basic concept of bosonic stimulation by atoms fails, whereas a simple picture of optical stimulation provides the correct answer (20).

References and Notes

1. R. H. Dicke, *Phys. Rev.* **93**, 99 (1954).
2. M. Gross, S. Haroche, *Phys. Rep.* **93**, 301 (1982).
3. W. Ketterle, S. Inouye, *Phys. Rev. Lett.* **86**, 4203 (2001).
4. M. G. Moore, P. Meystre, *Phys. Rev. Lett.* **86**, 4199 (2001).
5. S. Inouye et al., *Nature* **402**, 641 (1999).
6. M. Kozuma et al., *Science* **286**, 2309 (1999).
7. W. Ketterle, S. Inouye, in *Bose-Einstein Condensates and Atom Lasers*, A. Aspect, J. Dalibard, Eds., vol. IV of *Comptes Rendus de l'Académie des Sciences Paris* (Elsevier, Paris, 2001), pp. 339–380.
8. S. Inouye et al., *Science* **285**, 571 (1999).
9. M. G. Moore, P. Meystre, *Phys. Rev. Lett.* **83**, 5202 (1999).
10. Ö. E. Müstecaplıoğlu, L. You, *Phys. Rev. A* **62**, 063615 (2000).
11. N. Piovella, R. Bonifacio, B. W. J. McNeil, G. R. M. Robb, *Opt. Commun.* **187**, 165 (2001).
12. E. D. Trifonov, *J. Exp. Theor. Phys.* **93**, 969 (2001) [translation from E. D. Trifonov, *Zh. Eksp. Teor. Fiz.* **120**, 1117 (2001)].

13. P. J. Martin, B. G. Oldaker, A. H. Miklich, D. E. Pritchard, *Phys. Rev. Lett.* **60**, 515 (1988).
14. M. Kozuma et al., *Phys. Rev. Lett.* **82**, 871 (1999).
15. P. L. Gould, G. A. Ruff, D. E. Pritchard, *Phys. Rev. Lett.* **56**, 827 (1986).
16. Y. B. Ovchinnikov et al., *Phys. Rev. Lett.* **83**, 284 (1999).
17. For the 30-ms time of flight, the condensate expands by only 10% in the axial direction, as compared to more than a factor of 15 in the radial direction.
18. The fractional solid angle subtended by the condensate is $\Omega \sim (d^2/L^2)/4\pi$, where d is its diameter and L its length. The contribution of spontaneous Rayleigh

scattering to the endfire mode intensity thus is on the order of $\Omega \times (Nl_{sc}^2 \hbar \omega) \times 1/d^2 = 2.5 \times 10^{-3} \text{ m W cm}^{-2}$.

19. J. Stenger et al., *Phys. Rev. Lett.* **82**, 4569 (1999).
20. We would like to thank G. Campbell, A. Leanhardt, and J. Steinhauer for a critical reading of the manuscript and P. Meystre and S. Inouye for discussions. This work was supported by NSF.

7 February 2003; accepted 18 March 2003

Published online 27 March 2003;

10.1126/science.1083171

Include this information when citing this paper.

Mantle Fault Zone Beneath Kilauea Volcano, Hawaii

Cecily J. Wolfe,^{1*} Paul G. Okubo,² Peter M. Shearer³

Relocations and focal mechanism analyses of deep earthquakes (≥ 13 kilometers) at Kilauea volcano demonstrate that seismicity is focused on an active fault zone at 30-kilometer depth, with seaward slip on a low-angle plane, and other smaller, distinct fault zones. The earthquakes we have analyzed predominantly reflect tectonic faulting in the brittle lithosphere rather than magma movement associated with volcanic activity. The tectonic earthquakes may be induced on preexisting faults by stresses of magmatic origin, although background stresses from volcano loading and lithospheric flexure may also contribute.

Earthquake characteristics at the active Kilauea volcano have long been used to construct models of this shield volcano and to constrain the structure of its magmatic system (1–4). Based on hypocenters in the catalog of the U.S. Geological Survey Hawaiian Volcano Observatory (HVO) seismic network, it has been suggested that the earthquakes at Kilauea outline a pipe-like magma conduit that extends through the lithosphere to depths as great as 60 km (1–4), thereby delineating the magma pathway from its source to the surface. However, the accuracy of routinely determined hypocenters is limited by factors including the network geometry, the available arrival time picks, picking errors, and the presence of three-dimensional velocity heterogeneity. Thus, relocations of earthquakes, using relative location methods, which reduce the effects of velocity heterogeneity, combined with precise cross-correlation measurements, have produced more accurate locations (5–11) and delineated fault structures. Here, we present relocations of deep earthquakes, focusing on distinguishing magmatic versus tectonic events to understand how the growing volcano affects the crust and upper mantle.

Our data consist of waveforms from 1988 to 1998 in the catalog of routinely located deep earthquakes recorded by the HVO seismic network, amounting to 14,604 events spread across and around Hawaii. The voluminous Pu'u 'O'o-Kupaianaha eruption of Kilauea, which began in 1983 and still continues, was occurring throughout the study period. The seismic events at Kilauea can be classified into three types, (i) high-frequency earthquakes that indicate shear faulting, and (ii) long-period (LP) earthquakes and (iii) tremor (12, 13) that likely reflect resonance in fluid-filled conduits. The data set contains 2376 LP events, with 90% above 20-km depth, and 135 tremor events, with 90% below 30-km depth (14).

Precise arrival time differences for earthquake pairs were obtained using waveform cross correlation with parameters appropriate for high-frequency earthquakes (15), and these data were able to relocate 7034 hypocenters, or 48% of the analyzed events. This calculation is a minimum estimate of the number of similar events, because pairs will not correlate highly if the signal-to-noise ratio is low: small magnitude events that are displaced far from stations, such as small, deeper earthquakes, are more difficult to constrain. Families of highly correlated earthquakes occur when there are closely spaced clusters with similar focal mechanisms, as at fault zones. Hence, our relocated clusters identify fault zones in the lithosphere beneath Hawaii.

The subset of 2522 earthquakes relocated in the vicinity of Kilauea is shown in Figs. 1 and 2, and fig. S1 displays the total set of 7034

¹Hawaii Institute of Geophysics and Planetology, University of Hawaii at Manoa, Honolulu, HI 96822, USA.

²Hawaiian Volcano Observatory, U.S. Geological Survey, Hawaii National Park, HI 96718, USA. ³Scripps Institution of Oceanography, University of California at San Diego, La Jolla, CA 92093–0225, USA.

*To whom correspondence should be addressed. E-mail: wolfe@hawaii.edu